IPN Progress Report 42-179 • November 15, 2009

The Classical Capacity of Single-Mode Free-Space Optical Communication: A Review

Baris I. Erkmen*, Bruce E. Moision*, and Kevin M. Birnbaum*

We give a brief summary of the classical information capacity of single-mode free-space optical communication, both for pure-loss channels (i.e., with no background radiation), and for thermal-noise channels (i.e., with background radiation). We compare the capacities afforded by structured transmitters and receivers to that of the ultimate communication capacity. The ultimate capacity-achieving optical states are classical coherent states (i.e., ideal laser light), but the capacity-achieving receiver is yet to be determined. In addition, in photon-starved pure-loss channels, binary phase modulation in combination with the optimal receiver is near-capacity achieving, and more importantly, it is superior to on-off keying. In a pure-loss channel, heterodyne detection is near-optimal at high signal levels. In thermal-noise channels with high background noise and low signal we find that homodyne and heterodyne detection both approach the ultimate capacity, and at high signal heterodyne detection remains near-optimal. Finally, we quantify the degradation in channel capacity that is due to multiple noise modes contributing to the output of photon-counters.

Electromagnetic waves are fundamentally quantized, and they are governed by the laws of quantum mechanics [1, 2]. This quantized nature has long been observed at optical frequencies through high-sensitivity photodetection systems. Therefore, when optical fields are the physical information carrier in a communication link, the ultimate rate of reliable communication is dictated by noise sources of quantum mechanical origin. A fundamental premise of quantum mechanics, which distinguishes it from classical mechanics, is that the outcome of a measurement on an electromagnetic field is probabilistic, and the statistics of the outcome are determined both by the measurement performed, and the state of the electromagnetic field at the time of the measurement [3]. As a consequence, the rate of reliable communication is impacted by *both* the alphabet of optical states used to convey information, and the measurement at the receiver to extract this information from the information carrier.

In this article we address the capacity of a point-to-point communication channel utilizing optical fields as the physical information carrier. The mathematical framework that facilitates the analysis is (classical and

*Communication Architectures and Research Section.

The research described in this publication was carried out by the Jet Propulsion Laboratory, California Institute of Technology, under a contract with the National Aeronautics and Space Administration.

quantum) information theory and random coding theorems: namely Shannon's channel capacity theorem [4], and its quantum mechanical analog, the Holevo-Schumacher-Westmoreland (HSW) theorem [3]. A comprehensive survey of channel capacity results, with various technology-driven modulations, and using both classical and quantum receivers, has been reported in the recent literature [5, 6, 7, 8]. Our aim here is to complement this body of work by providing a summary of more recent results for single-mode free-space optical communication. We omit the derivations for brevity, and attempt to emphasize various avenues of future research that will enable communication at the ultimate rates dictated by quantum mechanics.

This article is organized as follows. We begin with a brief review of the fundamentals in Section I. In particular, we review the classical and quantum channel capacity theorems based on random coding, and the normal-mode decomposition of the free-space propagation channel, which justifies the concept of single-mode operation. We have organized the material such that during the first reading this section may be skipped with no loss in continuity. We review in Section II the capacity of the pure-loss propagation channel, and in Section III the capacity of a channel with background noise coupled in from the environment. In Section IV, we derive the asymptotic expressions for the ultimate channel capacity with and without background noise. The degradation due to multiple noise modes contributing to photon counting is considered in Section V. Finally, in Section VI we present conclusions derived from our summary, emphasizing potentially fruitful avenues for research and development to approach the ultimate channel capacity of free-space optical communication.

I. Preliminaries

Before we delve into a survey of various single-mode channel capacities, let us briefly review the foundation of these results. In Section I.A we first review Shannon's random channel coding theorem, and contrast this to its quantum counterpart, the HSW random coding theorem. Then, in Section I.B, we review free-space propagation for quasimonochromatic and paraxial optical beams and rigorously define a single-mode communication architecture.

We reiterate here that this section may be skipped in first reading, with no loss in continuity. It can be utilized as a reference section, and consulted as needed.

A. Random Coding Theorems: Classical and Quantum

In classical information theory, a discrete memoryless channel ε is described by a conditional probability map

$$\varepsilon \equiv \{p(y|x) : x \in \mathcal{X}, y \in \mathcal{Y}\} \tag{1}$$

where x is a symbol from the alphabet of input symbols $\mathcal{X}$, $y \in \mathcal{Y}$ is a symbol from the alphabet of output symbols $\mathcal{Y}$, and $p(y|x)$ is the probability that the output is y, given that x is the input. Shannon's well-known channel coding theorem [9] states that the maximum rate of reliable communication over a channel, i.e., the channel capacity C, is given by

$$C = \sup_{n \in \mathbb{N}^+} C_n/n \tag{2}$$

where

$$C_n = \max_{p(\mathbf{x}):\mathbf{x}\in\mathcal{X}^{\otimes n}} I\big(p(\mathbf{x}), \varepsilon^{\otimes n}\big) \tag{3}$$

is the n-use channel capacity.[1] In this expression, the maximization is carried out over all probability distribution functions defined on the alphabet space $\mathcal{X}^{\otimes n}$. The mutual information, $I\big(p(\mathbf{x}), \varepsilon^{\otimes n}\big)$, is between the n-tuples of random variables $\mathbf{X} = [X_1 \dots X_n]$ and $\mathbf{Y} = [Y_1 \dots Y_n]$, which can be expressed as follows for a discrete memoryless channel:

$$I\big(p(\mathbf{x}), \varepsilon^{\otimes n}\big) \equiv H\left(\sum_{\mathbf{x}\in\mathcal{X}^{\otimes n}} p(\mathbf{x}) \prod_{k=1}^{n} p(y_k|x_k)\right) - \sum_{\mathbf{x}\in\mathcal{X}^{\otimes n}} p(\mathbf{x}) H\left(\prod_{k=1}^{n} p(y_k|x_k)\right) \tag{4}$$

where

$$H\big(p(\mathbf{x})\big) = -\sum_{\mathbf{x}\in\mathcal{X}^{\otimes n}} p(\mathbf{x}) \ln\big(p(\mathbf{x})\big) \tag{5}$$

is the Shannon entropy of the probability distribution $p(\mathbf{x})$. In general, the maximization in Equation (3) would have to be carried out with respect to the joint probability density function for n input symbols, i.e., $p(\mathbf{x})$. However, because the mutual information for memoryless channels is known to be *additive* [9], the channel capacity for a discrete memoryless channel reduces to the single-use channel capacity

$$C = C_1 = \max_{p(x):x\in\mathcal{X}} I\big(p(x), \varepsilon\big) \tag{6}$$

which involves a simpler maximization over the marginal distribution $p(x)$.

Now let us turn to the quantum-mechanical analog of the random coding theorem. In quantum information theory, a memoryless channel ε is described by a completely-positive trace-preserving operator map $\varepsilon(\cdot)$

$$\varepsilon(\hat{\rho}_x) : \hat{\rho}_x \in \mathcal{H} \rightarrow \hat{\rho}_{y|x} \in \mathcal{H}' \tag{7}$$

where $\hat{\rho}_x$ is a density operator in the Hilbert space $\mathcal{H}$ indexed by x, and $\hat{\rho}_{y|x} \equiv \varepsilon(\hat{\rho}_x)$ is the output state (in the Hilbert space $\mathcal{H}'$) when $\hat{\rho}_x$ is the transmitted state. The HSW channel-coding theorem [3, 10, 19, 20] states that the maximum rate of reliable communication over this channel, i.e., the channel capacity C, is given by

$$C = \sup_{n\in\mathbb{N}^+} C_n/n \tag{8}$$

where

$$C_n = \max_{p(\mathbf{x}),\hat{\rho}_{\mathbf{x}}\in\mathcal{H}^{\otimes n}} \chi\big(p(\mathbf{x}), \hat{\rho}_{\mathbf{x}}, \varepsilon^{\otimes n}\big) \tag{9}$$

is the n-use channel capacity, and $\mathbf{x}$ is an index for states that reside in the n-tensor-product Hilbert space $\mathcal{H}^{\otimes n}$. Here, $\chi(p(\mathbf{x}), \hat{\rho}_{\mathbf{x}}, \varepsilon^{\otimes n})$ is the Holevo information between the joint state of n successive inputs to the

[1] Here we have departed from the standard notation, $I(X;Y)$, for the mutual information between two random variables X and Y, because it will facilitate a better analogy with the quantum case. In our notation, the first argument of the mutual information is the quantity to be maximized over and the second argument specifies the channel transformation. The mutual information is strictly a function of these two quantities.

channel and the joint state of the corresponding n outputs. The Holevo information is defined as

$$\chi(p(\mathbf{x}),\hat{\rho}_{\mathbf{x}};\varepsilon^{\otimes n}) \equiv S\left(\sum_{\mathbf{x}} p(\mathbf{x})\varepsilon^{\otimes n}(\hat{\rho}_{\mathbf{x}})\right) - \sum_{\mathbf{x}} p(\mathbf{x}) S\big(\varepsilon^{\otimes n}(\hat{\rho}_{\mathbf{x}})\big) \tag{10}$$

where

$$S(\hat{\rho}) = -\mathrm{tr}\big(\hat{\rho}\ln(\hat{\rho})\big) \tag{11}$$

is the von Neumann entropy of the density operator $\hat{\rho}$, which is equal to the Shannon entropy of its eigenvalues [3].[2] The maximization in Equation (9) is carried out with respect to $\hat{\rho}_{\mathbf{x}}$, i.e., the alphabet of joint states chosen from all possible states that can be transmitted over n uses of the channel (these states need not be product states), and $p(\mathbf{x})$, i.e., the classical probability distribution over this alphabet. The maximization over the alphabet set must be carried out because the state of the field at the receiver is one parameter that determines the outcome statistics, hence it affects channel capacity. The other parameter that determines the channel capacity is the measurement performed at the receiver. However, no explicit maximization over the measurement is needed, because the Holevo information is the rate achievable with the best possible measurement [10].

There has not been a proof to date that Holevo information is additive for memoryless channels, thus in general the cumbersome maximization over n, shown in Equation (8), is necessary. However, it turns out that the Holevo information for Bosonic pure-loss and thermal-noise channels is additive [11, 12]. Thus, for these channels we have

$$C = C_1 = \max_{p(x),\hat{\rho}_x\in\mathcal{H}} \chi\big(p(x),\hat{\rho}_x,\varepsilon\big) \tag{12}$$

i.e., the maximization is over the single-use Hilbert space and the associated marginal probability distribution.

B. Single-Mode Free-Space Propagation

Although the full-field paraxial free-space propagation of optical waves is governed by the Huygens-Fresnel principle [13, 14, 15], a communication channel utilizing a single optical field mode can be modeled as a simple beamsplitter. In this section we formally derive this equivalence.

Consider the paraxial line-of-sight geometry that is shown in Figure 1, where we have assumed that the propagation direction is along the z-axis. A quasimonochromatic scalar field with center-frequency ω_0 is transmitted through an aperture $\mathcal{A}_0$ on the $z=0$ plane and for a duration of T seconds. This field propagates through free space on a length-L line-of-sight path, and is received via the receiver aperture $\mathcal{A}_L$ on the $z=L$ plane. We denote the positive-frequency electric field operator that describes the transmitted field on the $z=0$ plane as $\hat{E}_0(\boldsymbol{\rho}',t)e^{j\omega_0 t}$, where $\hat{E}_0(\boldsymbol{\rho}',t)$ is the baseband operator that is excited (i.e., nonvacuum) only within domain $\boldsymbol{\rho}'\in\mathcal{A}_0$ and $t\in[0,T]$.

Throughout this article, we shall assume, for convenience, that $\hat{E}_0(\boldsymbol{\rho}',t)$ is normalized to photon units, i.e., it has units $\sqrt{\text{photons/m}^2\text{s}}$. This normalization is straightforward for a quasimonochromatic optical field, in which the frequency band that is excited is a very small fraction of the center frequency, so the energy of all

[2] In Equation (11), $\mathrm{tr}(\cdot)$ denotes the trace of the argument.

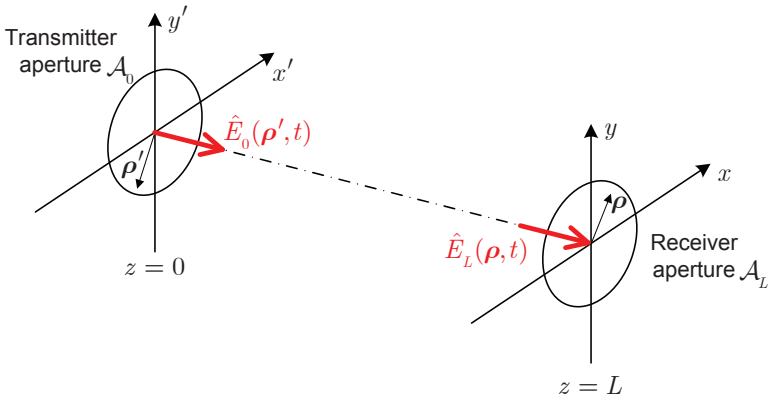

Figure 1. (Color online) A line-of-sight paraxial propagation geometry.

excited photons can be approximated as $\hbar\omega_0$, where $\hbar$ is 2π times Planck's constant. To obtain a photon-units field operator, the electric field operator, with units volt/$\sqrt{\text{m}^2\text{s}}$, is divided by $\sqrt{\hbar\omega_0\mu_0/2\epsilon_0}$, where $\sqrt{\mu_0/\epsilon_0} \approx 377\Omega$ is the characteristic impedance of vacuum[3] and the factor of $\sqrt{2}$ in the denominator is to account for the fact that half of the energy in an electromagnetic wave propagating in an isotropic medium is carried by the magnetic field. With this normalization, and in the quasimonochromatic paraxial approximation regime, $\hat{E}_0(\boldsymbol{\rho}', t)$ satisfies the canonical commutator relations [2]

$$[\hat{E}_0(\boldsymbol{\rho}'_1, t_1), \hat{E}_0(\boldsymbol{\rho}'_2, t_2)] = 0 \tag{13}$$

$$[\hat{E}_0(\boldsymbol{\rho}'_1, t_1), \hat{E}_0^\dagger(\boldsymbol{\rho}'_2, t_2)] = \delta(\boldsymbol{\rho}'_1 - \boldsymbol{\rho}'_2)\delta(t_1 - t_2)\,. \tag{14}$$

It is important to note that any valid transformation on a field operator (such as free-space diffraction) will preserve these commutator relations.

The diffraction of optical fields in free space is governed by the Huygens-Fresnel principle, in both the classical and quantum treatment of electromagnetism. In particular, the field operator at the $z = L$ plane, denoted by $\hat{E}_L(\boldsymbol{\rho}, t)$, is obtained from the transmitter-plane field operator as

$$\hat{E}_L(\boldsymbol{\rho}, t) = \int_{\mathcal{A}_0} \hat{E}_0(\boldsymbol{\rho}', t - L/c) h_L(\boldsymbol{\rho}, \boldsymbol{\rho}') \mathrm{d}\boldsymbol{\rho}' \tag{15}$$

where the Huygens-Fresnel Green's function is given by

$$h_L(\boldsymbol{\rho}, \boldsymbol{\rho}') \equiv \frac{\omega_0}{j2\pi cL} \exp\left\{ j\frac{\omega_0 L}{c} + j\frac{\omega_0}{2cL}|\boldsymbol{\rho} - \boldsymbol{\rho}'|^2 \right\} \tag{16}$$

In order to obtain a normal-mode decomposition of the communication channel, we consider the propagation

[3] μ_0 is the magnetic permeability of vacuum, and ϵ_0 is its dielectric permittivity.

kernel $h(\boldsymbol{\rho}, \boldsymbol{\rho}')$ over $\boldsymbol{\rho}' \in \mathcal{A}_0$ and $\boldsymbol{\rho} \in \mathcal{A}_L$, and perform a singular-value decomposition of the kernel, yielding

$$h_L(\boldsymbol{\rho}, \boldsymbol{\rho}') = \sum_{n=0}^{\infty} \sqrt{\eta_n} \phi_n(\boldsymbol{\rho}) \Phi_n^*(\boldsymbol{\rho}') \tag{17}$$

where $\{\Phi_n(\boldsymbol{\rho}') | n = 0, 1, \ldots; \boldsymbol{\rho}' \in \mathcal{A}_0\}$ is a complete and orthonormal (CON) set of input eigenfunctions, $\{\phi_n(\boldsymbol{\rho}) | n = 0, 1, \ldots; \boldsymbol{\rho} \in \mathcal{A}_L\}$ is the corresponding CON set of output eigenfunctions, and $\{\sqrt{\eta_n} | n = 0, 1, \ldots; \eta_n \geq 0\}$ are the associated singular values, which we assume—with no loss in generality—are listed in nonincreasing order. Let us also pick an arbitrary CON basis $\{\zeta_m(t) | m = 0, 1, \ldots\}$ on $t \in [0, T]$. Then, the input field operator at the $z = 0$ plane is fully described by

$$\hat{E}_0(\boldsymbol{\rho}', t) = \begin{cases} \sum_{n=0}^{\infty} \sum_{m=0}^{\infty} \hat{a}_{n,m} \Phi_n(\boldsymbol{\rho}') \zeta_m(t), & \text{for } (\boldsymbol{\rho}', t) \in \mathcal{A}_0 \times [0, T] \\ \hat{E}_{0,\text{aux}}(\boldsymbol{\rho}', t), & \text{for } (\boldsymbol{\rho}', t) \in (\mathbb{R}^2 - \mathcal{A}_0) \times [0, T] \end{cases} \tag{18}$$

where $\hat{a}_{n,m}$ are annihilation operators of a quantum harmonic oscillator, satisfying the commutation relations

$$[\hat{a}_{n,m}, \hat{a}_{n',m'}] = 0 \tag{19}$$

$$[\hat{a}_{n,m}, \hat{a}_{n',m'}^{\dagger}] = \delta_{n,n'} \delta_{m,m'} \tag{20}$$

and $\hat{E}_{0,\text{aux}}(\boldsymbol{\rho}', t)$ is an auxiliary field operator representing the field that lies *outside* of the transmitter aperture. As we shall see in the following sections, if no background noise is present this auxiliary field operator is in a vacuum state, but when background radiation is present $\hat{E}_{0,\text{aux}}(\boldsymbol{\rho}', t)$ is in an excited state.

Propagating the $z = 0$ field operator to the $z = L$ plane via Equation (15), and using the normal-mode decomposition in Equation (17) over the applicable domain, we find that the field operator on the $z = L$ plane, denoted by $\hat{E}_L(\boldsymbol{\rho}, t)$, is

$$\hat{E}_L(\boldsymbol{\rho}, t) = \sum_{n=0}^{\infty} \sum_{m=0}^{\infty} \hat{c}_{n,m} \phi_n(\boldsymbol{\rho}) \zeta_m(t - L/c) \tag{21}$$

for $(\boldsymbol{\rho}, t) \in \mathcal{A}_L \times [L/c, T + L/c]$, where we have

$$\hat{c}_{n,m} \equiv \sqrt{\eta_n} \hat{a}_{n,m} + \sqrt{1 - \eta_n} \hat{b}_{n,m} \tag{22}$$

Here $\hat{c}_{n,m}$ is the annihilation operator of the $(n, m)^{\text{th}}$ received field mode, in terms of the annihilation operator of the $(n, m)^{\text{th}}$ transmitted field mode $\hat{a}_{n,m}$, and the annihilation operator from the environment, $\hat{b}_{n,m}$. The environment modes are represented in terms of the auxiliary field operator at the transmitter plane as

$$\hat{b}_{n,m} \equiv \frac{1}{\sqrt{1 - \eta_n}} \int_0^T \int_{\mathcal{A}_L} \zeta_m^*(t) \phi_n^*(\boldsymbol{\rho}) \left[\int_{\mathbb{R}^2 - \mathcal{A}_0} h_L(\boldsymbol{\rho}, \boldsymbol{\rho}') \hat{E}_{0,\text{aux}}(\boldsymbol{\rho}', t) \mathrm{d}\boldsymbol{\rho}' \right] \mathrm{d}\boldsymbol{\rho} \mathrm{d}t \tag{23}$$

The receiver-aperture field operator expression given in Equation (21) corresponds to the parallel-channel model shown in Figure 2(a). The propagation channel can be decomposed into a (countably-infinite) set of decoupled subchannels, each of which is defined by the beamsplitter input-to-output relation given in Equation (22), and the corresponding mode functions. Furthermore, if we assume that the mode functions are known to both the

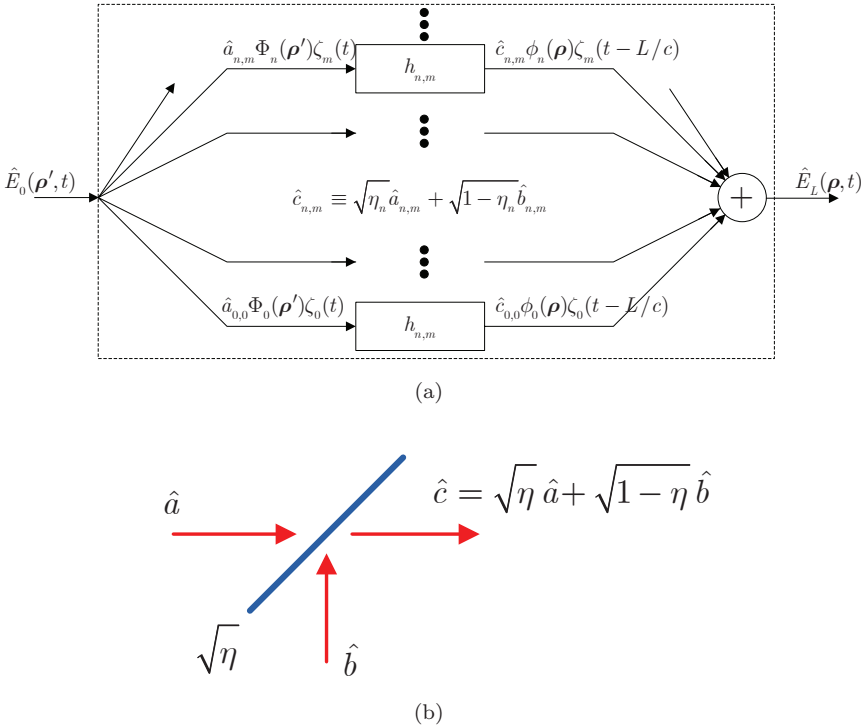

Figure 2. (Color online) (a) The parallel channel representation of quasimonochronimatic paraxial free-space propagation, and (b) the beamsplitter channel model for single-mode optical communication.

transmitter and the receiver, the communication channel is reduced to a set of beamsplitter relations. It is worthwhile to note that although we have demonstrated the principle of the normal-mode decomposition, obtaining the particular mode functions analytically may be nontrivial for arbitrary apertures. Nonetheless, analytic solutions are easy to obtain with soft Gaussian-attenuation apertures [14], and they can be obtained—in terms of prolate spherioidal functions—for hard circular apertures [16].

At this juncture, we can state in full rigor that a single-mode free-space communication channel is one in which the information transfer utilizes only one of the infinitely-many (n, m) modes at our disposal. The communication channel is therefore reduced to a single beamsplitter relation as shown in Figure 2(b), where we have suppressed the subscripts. Note that not all modes yield equal channel capacity, as the power coupling, η_n, is not the same for all of the available spatiotemporal modes of communication. Furthermore, although we limit the scope of this article to single-mode communication, the information capacity of this channel is maximized when the available average photon flux is optimally distributed over all available spatiotemporal modes [14].

In this article, we shall consider two scenarios: a pure-loss channel in which the environment, $\hat{b}$, is in the vacuum state, and a thermal-noise channel, in which the environment is in a thermal state.

II. The Pure-Loss Channel

As we have reviewed in Section I.B, a single-mode free-space optical communication channel can be modeled as a beamsplitter relation, which is depicted in Figure 2(b). Here, $\hat{a}$ denotes the input modal field operator—i.e., the annihilation operator—associated with the spatiotemporal mode that is utilized by the transmitter, $\hat{b}$ is the modal field operator for the environmental contribution (vacuum fluctuations or unwanted background radiation), and $\hat{c}$ is the output modal field operator at the receiver. The transmissivity of the beamsplitter, η, models the power coupling between the transmitted mode and the receiver.

In this section we shall take the environment mode, $\hat{b}$, to be in its vacuum state, and we impose a mean photon number constraint $\langle \hat{a}^\dagger \hat{a} \rangle \leq N_S$ on the transmitter.[4]

Ultimate capacity: The ultimate capacity of this channel, with no structural constraints imposed on the transmitter and receiver—other than the mean photon number constraint—is given by [11]

$$C_{\text{ult}} = g(\eta N_S) \,\text{nats/channel use} \tag{24}$$

where $g(x) = (1 + x)\ln(1 + x) - x\ln x$. It has been shown that this capacity may be achieved by *single-use coherent state encoding* with an isotropic Gaussian input probability density. In other words, messages are mapped to complex-valued codewords, wherein each entry in a codeword represents the complex amplitude of the transmitted laser pulse in the corresponding channel use. Analogous to the random-coding argument in Shannon's channel capacity theorem [9], the "optical codebook" is conceptually generated by choosing

[4] We denote ensemble averages throughout this article with angled-brackets. Thus, $\langle \hat{X} \rangle$ is the expected value of a measurement of the operator $\hat{X}$.

independent and identically distributed complex-valued entries, α, from an isotropic Gaussian distribution

$$p(\alpha) = \frac{1}{\pi N_S} e^{-|\alpha|^2/N_S} \tag{25}$$

Although the encoding strategy described above applies to all loss values $0 < \eta \leq 1$, the $\eta = 1$ case (i.e., the lossless channel) has historically received more attention [17, 6]. To that end, it is worth pointing out that when $\eta = 1$, an alternative encoding strategy is single-use number-state (i.e., Fock state) encoding with a Bose-Einstein prior. That is, the codewords are now chosen from an alphabet of nonnegative integers, wherein each entry indicates the number of photons that will be transmitted in the corresponding channel use. In quantum mechanics, the optical state that contains a deterministic number of photons is called a number state or a Fock state, which is nonclassical (the photodetection statistics of these states *cannot* be explained with shot noise theory). As in the coherent state case described above, a capacity-achieving codebook can be generated (with high probability) by choosing independent and identically distributed entries from the Bose-Einstein (geometric) distribution

$$p(n) = \frac{N_S^n}{(1+N_S)^{n+1}}, \quad n = 0, 1, 2, \ldots \tag{26}$$

Thus far, we have only considered encoding strategies. Unfortunately, much less can be said about the optimal measurement (i.e., receiver), because the quantum analog of the channel coding theorem implicitly maximizes over all possible measurements. It is known mathematically that a square-root measurement can be used for decoding [3, 18]; however, the level of abstraction implied by this measurement is similar to that of maximum-likelihood or jointly-typical decoding in Shannon's channel coding theorem. Consequently, to this date, a physical realization of the capacity-achieving receiver for the pure-loss channel *has not been determined*. However, it is expected that the optimal receiver for coherent-state encoding performs measurements over multiple channel uses [19, 20].

It should be noted that capacity-achieving state alphabets may not be unique, i.e., a different set of transmitter states (in combination with a different set of prior probabilities and a different measurement at the receiver), could achieve capacity as well. These different coding possibilities may have different error exponents, and may have different decoding complexities. For example, in the $\eta = 1$ (lossless) case, number-state encoding, with a simple symbol-by-symbol photon-counting measurement (realized by an ideal photodetector) achieves the ultimate channel capacity. Furthermore, number-state encoding combined with photon-counting is error free for finite-length codewords, whereas coherent-state encoding is only error free in the asymptotic limit of infinite length codewords. Nonetheless, number-state encoding and photon counting no longer achieve capacity when $\eta < 1$, whereas coherent-state encoding remains optimal.

We shall consider the capacity of structured transmitter and receivers next. However, before we move on, it is important to emphasize that the ultimate-capacity-achieving transmitter is *classical*. It requires a phase and amplitude stable laser; however, no nonclassical states are required. The receiver, on the other hand, may have high complexity because multiple-symbol measurements (over multiple channel uses) are likely to be necessary [21, 22].

Coherent-state encoding and homodyne detection: Homodyne detection is a coherent detection technique in

which a strong local oscillator and a weak incoming field are mixed on a beamsplitter prior to photodetection [23, 24, 25]. In homodyne detection, the center frequency of the local oscillator and that of the signal field are identical, which facilitates the measurement of a single quadrature of the incident field. Quantum mechanically, homodyne detection corresponds to a measurement of one quadrature of the annihilation operator $\hat{c}$, and the quadrature that is measured can be altered by adjusting the phase of the local oscillator, θ_{LO} [1]. If the transmitted field operator, $\hat{a}$, is in a coherent state $|\alpha\rangle$, with $\alpha \in \mathbb{C}$, then the measurement outcome is a real-valued Gaussian random variable with mean $\sqrt{\eta}\Re\{\alpha e^{-j\theta_{\text{LO}}}\}$, and variance 1/4. We therefore have an additive white Gaussian noise channel, with the capacity [9]

$$C_{\text{coh-hom}} = \frac{1}{2}\ln(1 + 4\eta N_S) \text{ nats/channel use} \tag{27}$$

This capacity is achieved by choosing $\alpha = Xe^{j\theta_{\text{LO}}}$, where X is a real-valued Gaussian random variable with zero mean, and variance N_S.

Coherent-state encoding and heterodyne detection: Heterodyne detection is a coherent detection technique in which the local oscillator is frequency-shifted from the incoming field by an electronically detectable amount. This facilitates the measurement of both the real and imaginary quadratures of the incident field, at the expense of adding image-band noise [23, 24, 25]. Quantum mechanically, heterodyne detection yields complex-valued measurement outcomes that correspond to the measurement of the annihilation operator $\hat{c}$.[5] If $\hat{a}$ is in a coherent state $|\alpha\rangle$, with $\alpha \in \mathbb{C}$, then the measurement outcome is a complex-valued Gaussian random variable with mean $\sqrt{\eta}\alpha$, and variance 1. We therefore have a complex-valued, additive, white and isotropic Gaussian noise channel, with the capacity [9]

$$C_{\text{coh-het}} = \ln(1 + \eta N_S) \text{ nats/channel use} \tag{28}$$

This capacity is achieved by choosing α from the same isotropic Gaussian distribution given in Equation (25). To that end, it is a good example of the degradation in performance when optimal encoding (modulation), but suboptimal decoding (measurement) is used.

On-off keying (with coherent states) and direct detection: Here, we consider coherent-state encoding and a photon-counting measurement $\hat{N} = \hat{c}^\dagger\hat{c}$. If $\hat{a}$ is in a coherent state $|\alpha\rangle$, with $\alpha \in \mathbb{C}$, then the measurement outcome is a Poisson distributed random variable with mean value $\eta|\alpha|^2$. Unfortunately (and surprisingly), the capacity of the discrete-memoryless Poisson channel is still an open problem [28]. So we shall restrict ourselves to a particular modulation, namely on-off keying (OOK). It is known that when $\eta N_S \ll 1$, OOK approaches the ultimate channel capacity [Equation (24)], and therefore becomes near-optimal [29].

The only source of error in coherent-state OOK and photon counting over a pure-loss channel is when a pulse is transmitted, but no photon is registered, i.e., it is a Z-channel with probability of error $\varepsilon(p) = e^{-\eta N_S/p}$, where p is the probability of transmitting a pulse. Therefore the capacity is

$$C_{\text{OOK-pc}} = \max_{p\in[0,1]} h_2\Big(p\big(1-\varepsilon(p)\big)\Big) - p\, h_2\big(\varepsilon(p)\big) \text{ nats/channel use} \tag{29}$$

where $h_2(\varepsilon) = -\varepsilon\ln\varepsilon - (1-\varepsilon)\ln(1-\varepsilon)$ is the binary entropy function. The maximization over p requires solving

[5] Because $\hat{c}$ is not a Hermitian operator, this is a probability operator-valued measure (POVM) with differential eigenkets $\mathrm{d}^2\alpha|\alpha\rangle\langle\alpha|/\pi$ [26, 27].

transcendental equations, so we resort to numerical maximization.

On-off keying (with coherent states) and optimal receiver: Let us restrict our modulation to OOK with coherent states, but allow an arbitrary receiver. The Holevo information in Equation (10) represents the maximum rate of reliable communication optimized over all receivers [3]. Therefore, the channel capacity for coherent-state OOK is given by

$$C_{\text{OOK-ult}} = \max_{p\in[0,1]} h_2\left(\frac{1}{2}\left[1+\sqrt{1-4p(1-p)(1-e^{-\eta N_S/p})}\right]\right) \text{ nats/channel use} \tag{30}$$

where p represents the probability of the 'on' state, and $h_2(\cdot)$ is the binary entropy function defined earlier. Carrying out the maximization with respect to p requires solving for the root of the transcendental equation

$$p(1-2p) - \big(p(1-2p) + (1-p)\eta N_S\big)e^{-N_S/p} = 0 \tag{31}$$

which is carried out numerically.

Binary Phase-Shift Keying (with coherent states) and the Dolinar receiver: Let us now consider a phase modulation, where a coherent state with amplitude $\sqrt{N_S}$ is transmitted with probability p, and a coherent state with amplitude $-\sqrt{N_S}$ is transmitted with probability $1-p$. We will consider a symbol-by-symbol measurement that minimizes the probability of error in distinguishing between these two states, namely the Dolinar receiver [30]. This yields a binary symmetric channel with the crossover probability, ϵ, given by

$$\epsilon = (1-\sqrt{1-e^{-4\eta N_S}})/2 \tag{32}$$

Thus, the channel capacity for BPSK modulation and a Dolinar receiver is

$$C_{\text{BPSK-Dol}} = \ln 2 - h_2(\epsilon) \text{ nats/channel use} \tag{33}$$

This capacity is achieved with $p = 1/2$.

Binary Phase-Shift Keying (with coherent states) and optimal receiver: Let us consider the same phase modulation as before: a coherent state with amplitude $\sqrt{N_S}$ is transmitted with probability p, and a coherent state with amplitude $-\sqrt{N_S}$ is transmitted with probability $1-p$. Maximizing the Holevo information with respect to p yields [29]

$$C_{\text{BPSK-ult}} = h_2\left(\frac{1}{2}\left[1+e^{-2\eta N_S}\right]\right) \text{ nats/channel use} \tag{34}$$

This capacity is achieved with $p = 1/2$.

In Figure 3, all of the aforementioned capacities are plotted as a function of the mean signal photon number at the receiver, ηN_S. Figure 4 plots the same information as a function of the photon cost (defined as the mean photon number divided by the channel capacity) and the symbol cost (defined as the multiplicative inverse of the channel capacity) [31]. In this latter figure, the desired regime of operation is the bottom left corner, which corresponds to photon-efficient and bandwidth-efficient communication.

The ultimate capacity, as expected, outstrips all of the capacity curves obtained with structured transmitters or

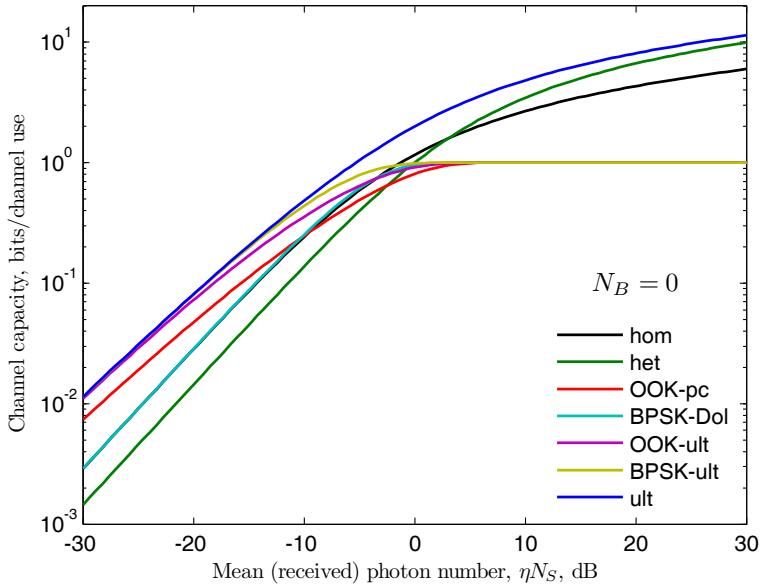

Figure 3. (Color online) Ultimate channel capacity of a pure-loss optical communication channel and the capacities achieved by structured transmitter and receivers.

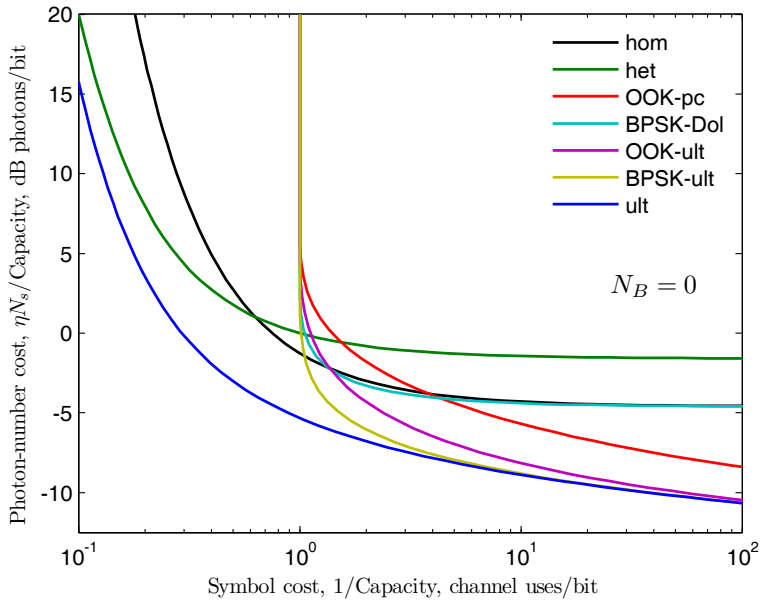

Figure 4. (Color online) The ultimate capacity of a pure-loss channel and the capacities of structured transmitter and receivers plotted in terms of symbol cost and photon-number cost.

receivers. All binary modulations are limited to at most ln2 nats/channel use, therefore they are useful in photon-starved links (i.e, links with $\eta N_S \ll 1$). In this regime, BPSK combined with the optimal receiver performs very close to the ultimate capacity. OOK, in combination with the optimal receiver, also closely tracks the ultimate capacity, although this capacity is strictly lower than that of BPSK with its optimal receiver. A noteworthy difference between the two modulations, however, is the peak-to-average photon-flux ratio. For BPSK this ratio is unity, whereas for OOK it is $1/p$, i.e., the multiplicative inverse of the duty cycle. The optimal duty cycles for OOK (with the optimal receiver and with photon-counting) are shown in Figure 5, as a function of ηN_S. When $\eta N_S < 1$, the peak-to-average photon flux is much greater than unity. Consequently, as ηN_S decreases, a practical OOK optical transmitter would become limited by its peak photon flux, whereas a BPSK transmitter does not suffer from this limitation.

OOK in combination with photon-counting is often considered a near-optimal configuration. Indeed, Figure 3 shows that as ηN_S decreases, the capacity of this configuration asymptotically approaches both the capacity of OOK with the optimal receiver, and the ultimate capacity. Figure 4 shows a similar convergence in symbol cost (the number of channel uses per information bit) as the photon-number cost (the mean number of received photons per information bit) goes to zero. However, in either plot the convergence occurs very slowly. This slow rate of convergence is apparent in Figure 6, in which we have plotted the ratio of each capacity to the ultimate capacity. For example, at $\eta N_S = 0.1$, the ratio of the OOK plus photon-counting capacity to the ultimate capacity is 1/2, and at $\eta N_S = 0.001$, this ratio is approximately 2/3. Another difference between OOK with photon-counting and OOK with the optimal receiver is their capacity-achieving peak-to-average photon fluxes. In particular, the peak-to-average photon-flux ratio required by the optimal receiver is notably smaller than that required by photon counting, when $\eta N_s \ll 1$. For example, from Figure 5 we see that at $\eta N_S = 0.01$, the peak-to-average photon flux with the former receiver is approximately four times smaller than that with the photon-counting receiver. However, it is worthwhile to reiterate that both configurations yield high peak-to-average photon-flux ratios in comparison to phase modulations, such as BPSK.

The Dolinar receiver is known to be the symbol-by-symbol optimal (i.e., minimum probability of symbol error achieving) receiver for BPSK [30], therefore, one might be inclined to expect that its capacity is near-optimal. However, this is not so, as its performance is significantly worse than BPSK with the optimal receiver. Figure 4 shows that BPSK plus the Dolinar receiver has a minimum symbol cost due to its binary alphabet, and a minimum photon cost due to single-symbol errors that dominate the performance in the $\eta N_S \ll 1$ regime.

The capacities of the two coherent receivers, i.e., homodyne and heterodyne detection, intersect when the channel transitions from the photon-number-limited regime into the bandwidth limited regime. In particular, at low photon numbers communication is limited by the quantum noise of the measurement (or the local-oscillator shot noise in the semiclassical interpretation), so homodyne detection outperforms heterodyne detection due to its higher signal-to-noise ratio. On the other hand, at high photon numbers, when the channel is bandwidth constrained, heterodyne detection outperforms homodyne detection, because it measures more degrees of freedom of the complex optical field, i.e., heterodyne detection measures both quadratures of the incident field, whereas homodyne is limited to a single quadrature.[6] We show in Section IV that at high signal mean photon

[6]The homodyne versus heterodyne detection performance tradeoff can be thought of as follows: Homodyne detection yields one real-valued additive Gaussian noise channel. Heterodyne detection, on the other hand, yields two real-valued additive Gaussian noise channels, but each has half the SNR of the former. When photon-number constrained, it is better to use the single channel with the higher SNR, whereas when bandwidth constrained, it is better to use the two channels offered by heterodyne detection.

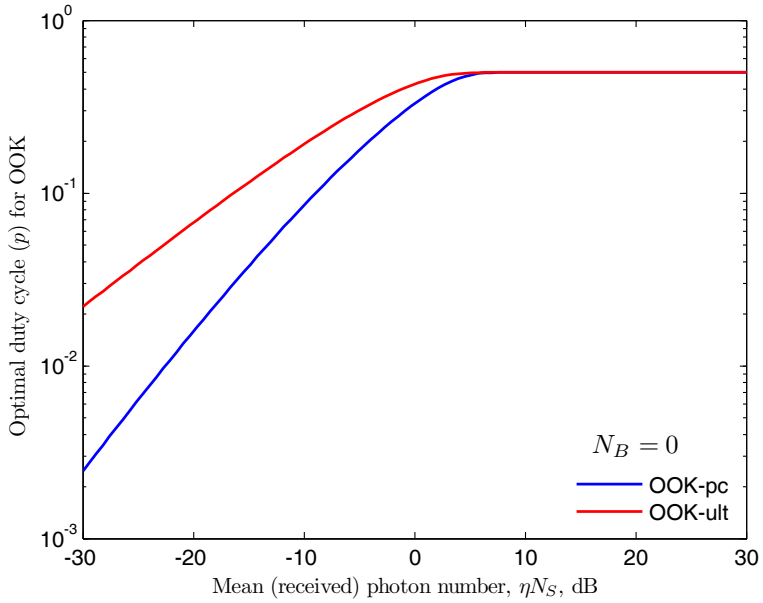

Figure 5. (Color online) The optimal duty cycle for OOK modulation.

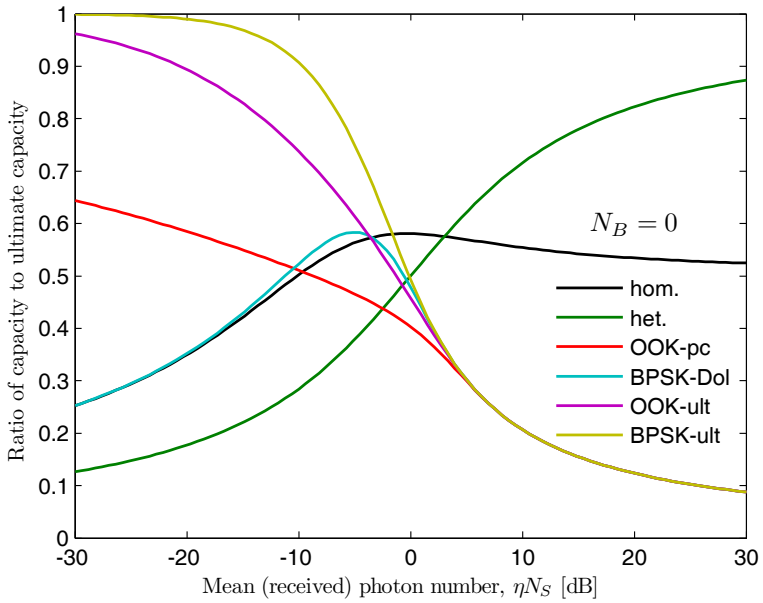

Figure 6. (Color online) Ratio of channel capacities with structured transmitter and receivers, to the ultimate capacity.

numbers heterodyne detection approaches the ultimate channel capacity, which can be visually verified from Figure 6.

III. The Thermal-Noise Channel

We now introduce background radiation by letting the environment mode $\hat{b}$ be in a thermal state (zero-mean Gaussian state) with mean photon number $\langle \hat{b}^\dagger \hat{b} \rangle = N_B$. We continue to impose a mean photon number constraint $\langle \hat{a}^\dagger \hat{a} \rangle \leq N_S$ on the transmitter.

The mean photon number of background radiation that occupies each spatiotemporal mode at optical frequencies is given by [32]

$$N_B = \frac{10^6 \lambda_0^5 S}{2c^2 h} \tag{35}$$

where S is the background spectral radiance specified in $\mathrm{W/m^2Sr}\mu\mathrm{m}$, λ_0 is the central wavelength, c is the speed of light in vacuum, and h is Planck's constant. In the near-infrared (IR) regime, which is of most interest to current optical communications, N_B is dominated by scattered sunlight, and assumes values that are very small fractions of a photon. For example, at $\lambda_0 = 1.55\,\mu$m, S can range from 10 to 1000 (in $\mathrm{W/m^2Sr}\mu\mathrm{m}$) [32], which yields N_B values that range from 10^{-8} to 10^{-5} photons per mode [32]. As evidenced by the capacity formulas that will be presented in this section, the impact of such small numbers of noise photons is negligible, because most (if not all) optical communication links are designed to operate with significantly higher mean signal photon number. Consequently, there is little loss in accuracy in using the pure-loss channel capacity results from the previous section, in order to determine the channel capacity of free-space optical communication links.

However, not all communication links operate within the near-IR band, or operate in noise conditions that are dominated by scattered sunlight. For example, it has been shown that atmospheric absorption and scattering is low in the $8\,\mu$m-to-$15\,\mu$m window [32], which makes it desirable for communication. The noise in this band is limited by blackbody radiation, which ranges from 10^{-2} to 1 photon per mode at room temperature, as shown in Figure 7. In addition, the Sun radiates approximately 0.25 photons per mode in the near-IR range, which can dominate the noise seen by an optical communication receiver that is pointing close to the Sun (this is a routine consideration in designing deep-space optical communications). If the center wavelength of interest is moved out to the $10\,\mu$m to $1000\,\mu$m range, which corresponds to *terahertz* frequencies (mid-IR and far-IR range of the electromagnetic spectrum) [33, 34], blackbody radiation at room temperature varies between 1 to 10 photons per mode. In this section, in order to cover communication performance results that span a broad range of background conditions, we shall show plots for $N_B = 1$ and $N_B = 10$, with the understanding that for $N_B \ll 1$, the pure-loss channel capacity results are good approximations to performance.

Ultimate capacity: The ultimate capacity of the thermal-noise channel, with no structural constraints imposed on the transmitter and receiver, is given by [12, 14]

$$C_{\mathrm{ult}}^{(\mathrm{th})} = g\big(\eta N_S + (1-\eta)N_B\big) - g\big((1-\eta)N_B\big) \text{ nats/channel use} \tag{36}$$

where $g(x)$ was defined in the previous section. This is in fact the maximum rate achievable with single-use coherent state encoding where the symbols are drawn from an isotropic Gaussian probability distribution. The

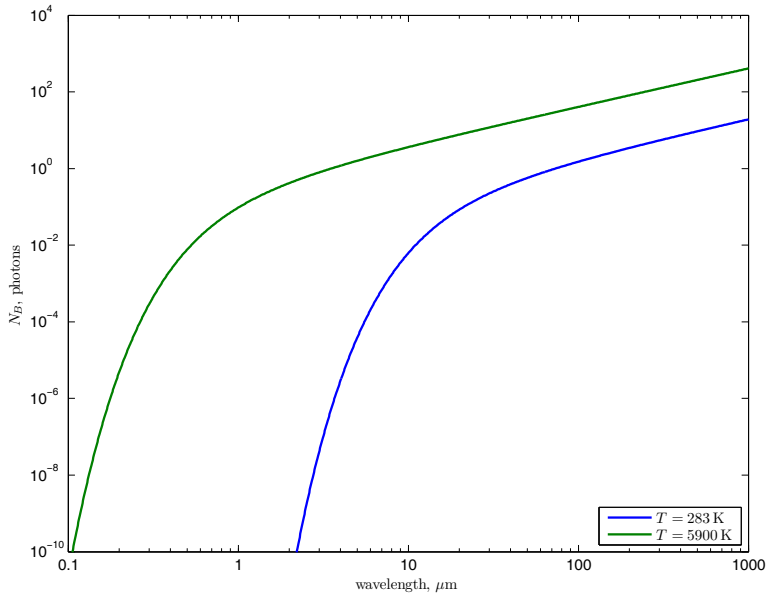

Figure 7. (Color online) Blackbody radiation per mode at room temperature ($283\,\mathrm{K}$) and that from the Sun (at $5900\,\mathrm{K}$).

converse of this statement, i.e., that communicating at a rate higher than $C_{\text{ult}}^{(\text{th})}$ yields a probability of error bounded away from zero, was initially posed as a conjecture, the truth of which hinged on proving the "minimum output entropy conjecture" for a beamsplitter [35]. This conjecture was later shown to be a special case of the "Entropy Photon-Number inequality conjecture" [36]. However, recently all of these conjectures have been proven true [37, 38]. Thus, $C_{\text{ult}}^{(\text{th})}$ is the capacity of the thermal-noise channel. As with the pure loss channel, a physical realization of the capacity-achieving receiver for the thermal-noise channel is not yet determined. Nonetheless, the ultimate capacity is achievable by transmitting only classical states of light.

Coherent-state encoding and homodyne detection: When $\hat{a}$ is in a coherent state $|\alpha\rangle$, with $\alpha \in \mathbb{C}$, a homodyne measurement yields a real-valued Gaussian random variable with mean $\sqrt{\eta}\Re\{\alpha e^{-j\theta_{\text{LO}}}\}$, and variance $(1-\eta)N_B/2 + 1/4$. Hence, the capacity is given by [36]

$$C_{\text{coh-hom}}^{(\text{th})} = \frac{1}{2}\ln\left(1 + \frac{4\eta N_S}{2(1-\eta)N_B + 1}\right) \text{ nats/channel use} \tag{37}$$

This capacity is, once again, achieved with $\alpha = Xe^{j\theta_{\text{LO}}}$, where X is a real-valued Gaussian random variable with mean zero and variance N_S, and θ_{LO} is the local oscillator phase.

Coherent-state encoding and heterodyne detection: When $\hat{a}$ is in a coherent state $|\alpha\rangle$, with $\alpha \in \mathbb{C}$, a heterodyne measurement yields a complex-valued Gaussian random variable with mean $\sqrt{\eta}\alpha$, and variance $(1-\eta)N_B + 1$. We therefore have a complex-valued additive white Gaussian noise channel, with the capacity [36]

$$C_{\text{coh-het}}^{(\text{th})} = \ln\left(1 + \frac{\eta N_S}{(1-\eta)N_B + 1}\right) \text{ nats/channel use} \tag{38}$$

This capacity is achieved by choosing α, once again, from an isotropic complex-valued Gaussian distribution

with zero mean and variance N_S.

On-off keying (with coherent states) and photon-counting: Let us return to coherent-state encoding and a photon-counting receiver. In particular, the transmitter chooses the coherent state $|\sqrt{N_S/p}\rangle$ with probability p, and the vacuum state $|0\rangle$ with probability $1-p$. When a pulse is transmitted, the received optical field operator $\hat{c}$ is in a displaced thermal state with mean $\sqrt{\eta N_S/p}$ and conditional variance $(1-\eta)N_B$. When no pulse is transmitted, $\hat{c}$ is in a thermal state with zero mean and conditional variance $(1-\eta)N_B$.

The photon-counting measurement on a field mode that is in a displaced thermal state with mean $\alpha \in \mathbb{C}$ and variance N_B yields an outcome with the probability mass function [2, 24, 39],

$$p(n) = \frac{N_B^n}{(1+N_B)^{n+1}} L_n\left(\frac{-|\alpha|^2}{N_B(1+N_B)}\right) e^{-|\alpha|^2/(1+N_B)} \tag{39}$$

for $n = 0, 1, 2, \ldots$, where $L_n(x)$ is a Laguerre polynomial of order n. Note that when $\alpha = 0$, the distribution simplifies to the Bose-Einstein distribution, which is the photon-counting distribution due to a thermal state. In addition, using the limit $\lim_{x\to 0} x^n L_n(-a/x) = a^n/n!$, we observe that in the $N_B \to 0$ limit Equation (39) converges to a Poisson distribution, which is the photon-counting distribution due to a coherent-state field mode.

The channel capacity for coherent-state OOK is a one-dimensional optimization of the mutual information over the pulse transmission probability $p \in (0, 1]$. Nonetheless, the mutual information for a given p is not known in closed form. Thus the maximization over p must be carried out numerically.

In Figure 8, we have plotted the capacities considered thus far as a function of the mean signal photon number at the receiver, ηN_S, for mean received noise photon numbers $(1-\eta)N_B = 1$ and $(1-\eta)N_B = 10$. Figure 9 is a plot of the symbol cost (the multiplicative inverse of the capacity) versus the photon-number cost (ηN_S divided by the capacity) for each of the capacities considered in this section. We observe from these two figures that heterodyne and homodyne detection both outperform OOK with photon counting. Furthermore, as we will show in the next section, when $\eta N_S \ll (1-\eta)N_B$ and $(1-\eta)N_B \gg 1$, the homodyne and heterodyne detection channel capacities approach ultimate capacity of the channel. In this regime homodyne detection performs marginally better than heterodyne detection due to a marginal advantage in the signal SNR. In the opposite end of the spectrum, when $\eta N_S \gg (1-\eta)N_B$, heterodyne detection is near optimal. In this high signal regime, homodyne detection suffers some loss from measuring one quadrature of the received field, whereas heterodyne detection affords higher throughput by facilitating information transmission over both quadratures of the field. The asymptotic performance of the coherent detection schemes mentioned above is captured in the ratio of their channel capacities to the ultimate capacity, which is plotted in Figure 10. When $(1-\eta)N_B = 10$, heterodyne detection yields a capacity greater than $0.95 C_{\text{ult}}^{(\text{th})}$ for all ηN_S.

The poor performance of OOK plus photon counting relative to that of coherent (homodyne or heterodyne) detection is clear in Figures 9 and 10. An additional challenge in utilizing OOK plus photon counting is the very high peak-to-average photon-flux ratio required by this modulation scheme. In particular, Figure 11 plots the optimal duty cycle for OOK, which is the multiplicative inverse of the peak-to-average photon flux. We observe that at $\eta N_S = 0.1$, the capacity-achieving peak-to-average photon flux ratio is approximately 100 for $(1-\eta)N_B = 1$, and 1000 for $(1-\eta)N_B = 10$.

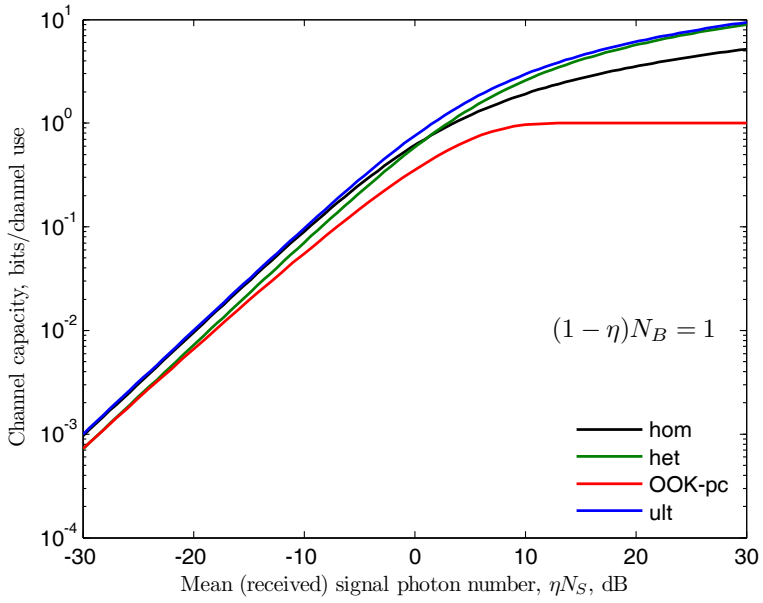

(a) $(1-\eta)N_B = 1$.

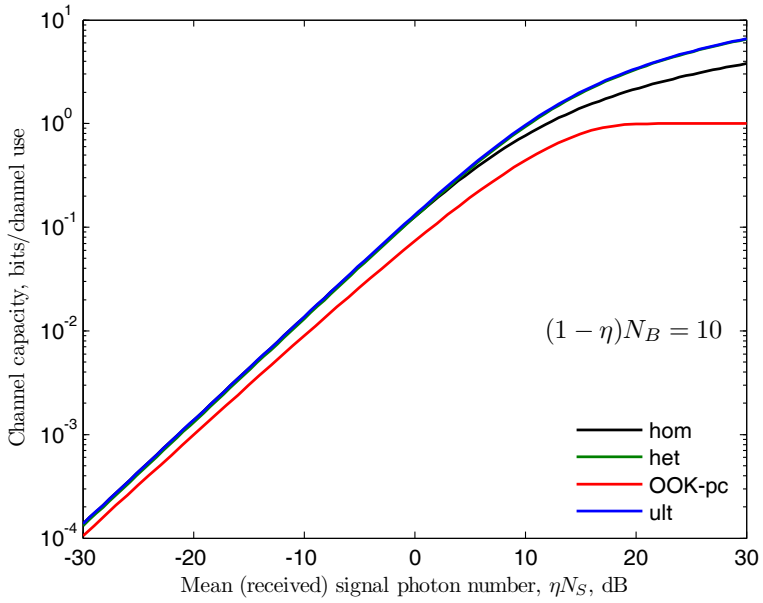

(b) $(1-\eta)N_B = 10$.

Figure 8. (Color online) The channel capacity of a thermal-noise optical communication channel and the capacities achieved by coherent detection.

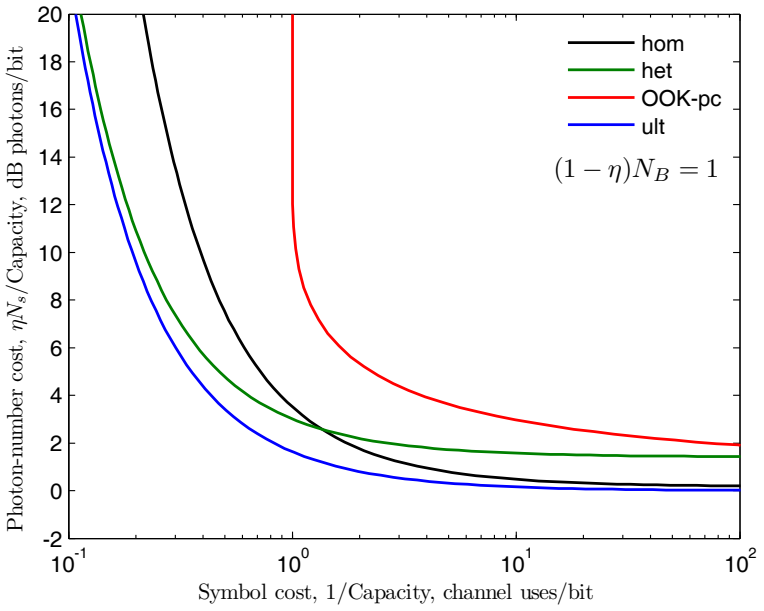

(a) $(1-\eta)N_B = 1$.

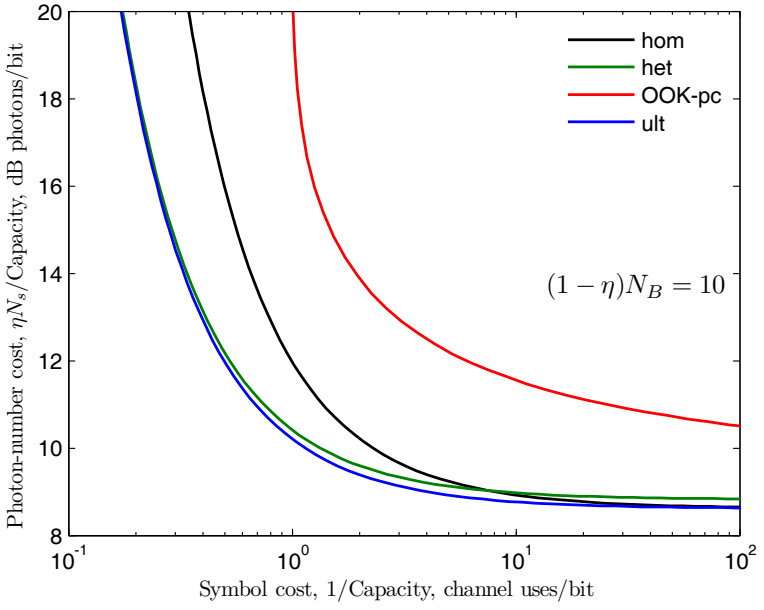

(b) $(1-\eta)N_B = 10$.

Figure 9. (Color online) The ultimate capacity of a thermal-noise channel and the capacities of structured transmitter and receivers are plotted in terms of symbol cost and photon-number cost.

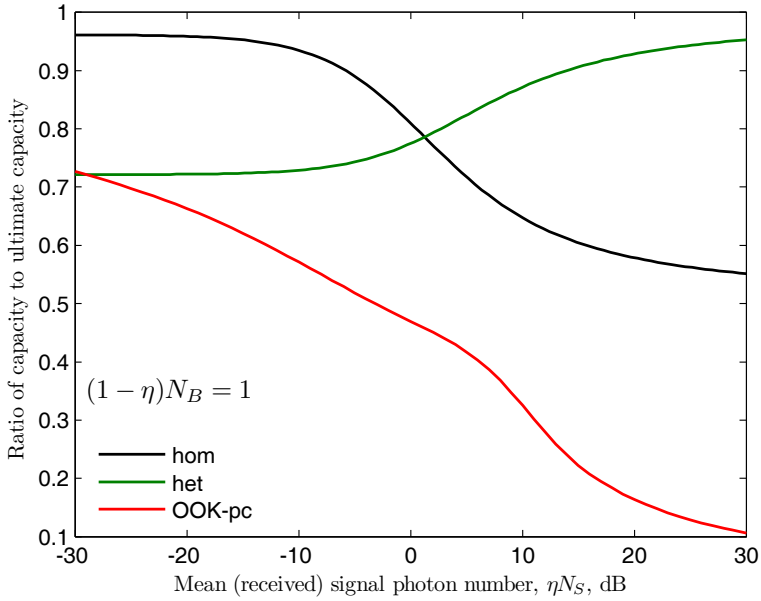

(a) $(1-\eta)N_B = 1$.

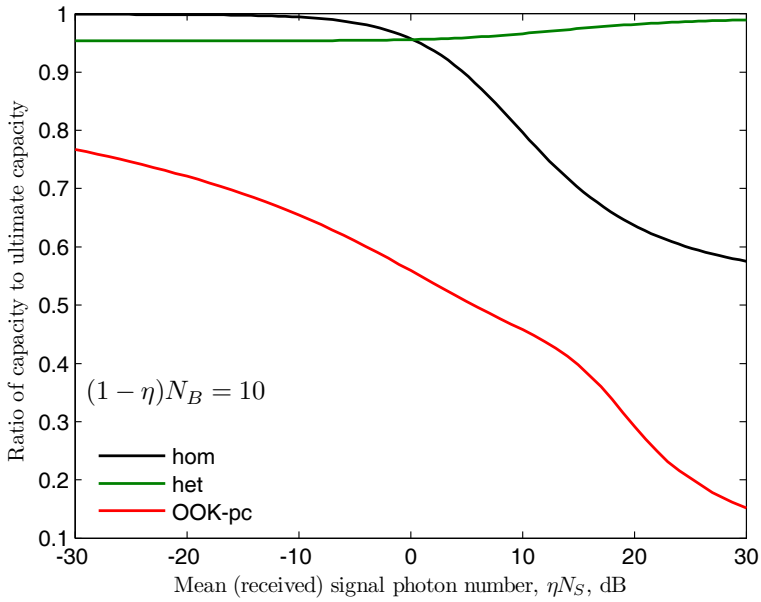

(b) $(1-\eta)N_B = 10$.

Figure 10. (Color online) Ratio of channel capacities with coherent detection receivers, to the ultimate capacity.

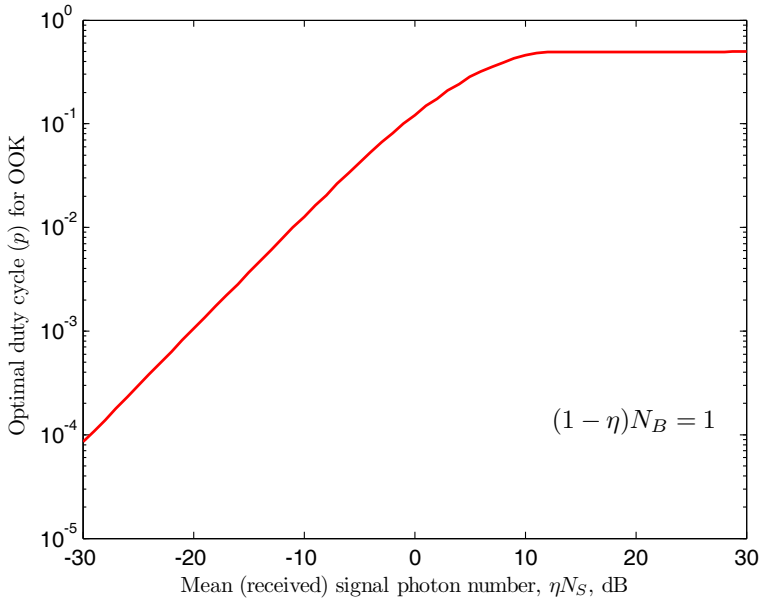

(a) $(1-\eta)N_B = 1$.

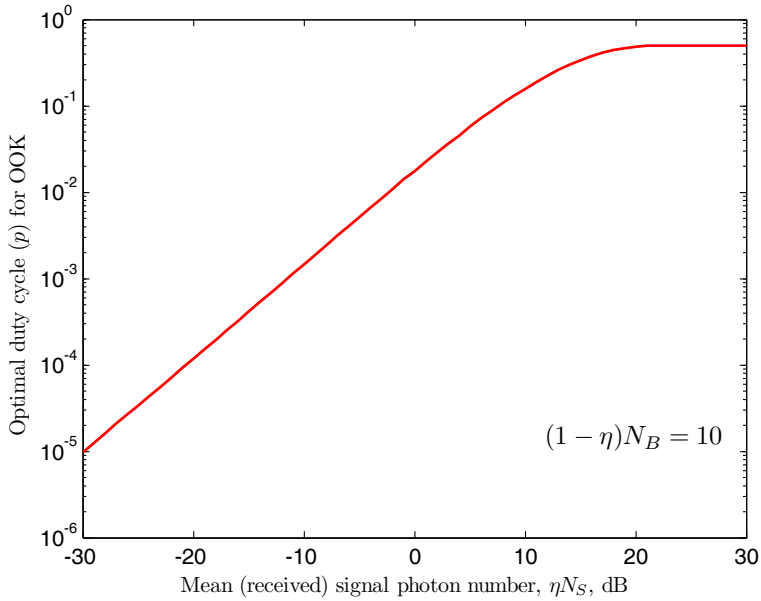

(b) $(1-\eta)N_B = 10$.

Figure 11. (Color online) Numerically-evaluated optimal duty cycle for OOK modulation and photon-counting photodetection.

Before concluding, it is worth reiterating here what we have established at the beginning of this section. Free-space optical links that operate in the near-IR and do not point close to the Sun will have a single-mode communication performance almost as good as the pure-loss channel. A mean background photon number of 1 per mode is possible if the sun is within the field of view, or if the communication frequency is on the order of tens of micrometers (mid-IR range). A mean background photon number of 10 is very much above the nominal values seen in near-IR optical frequencies, and is more applicable to the far-IR and the terahertz frequency range.

IV. Asymptotic Expressions for the Ultimate Capacity

Here we shall give expressions for the asymptotic behavior of the ultimate capacity. Recall from Equation (36) that the ultimate capacity is given by

$$C_{\text{ult}}^{(\text{th})} = g(n_s + n_b) - g(n_b) \tag{40}$$

where, $g(x) \equiv (1+x)\ln(1+x) - x\ln(x)$, and, for convenience of notation, we have used $n_s \equiv \eta N_S$ and $n_b \equiv (1-\eta)N_B$. When $n_b > 0$ and $n_s \ll n_b$, we can write[7]

$$C_{\text{ult}}^{(\text{th})} = n_s \ln(1 + 1/n_b) + o(n_s/n_b) \tag{41}$$

Therefore, using the expressions from Equation (37) and Equation (38), we find that

$$\frac{C_{\text{coh-hom}}^{(\text{th})}}{C_{\text{ult}}^{(\text{th})}} = \frac{1}{(n_b + 1/2)\ln(1 + 1/n_b)} \tag{42}$$

and

$$\frac{C_{\text{coh-hom}}^{(\text{th})}}{C_{\text{ult}}^{(\text{th})}} = \frac{1}{(n_b + 1)\ln(1 + 1/n_b)} \tag{43}$$

for $n_s \ll n_b$. If, in addition, $n_b \gg 1$ holds, we have $\ln(1 + 1/n_b) \approx 1/n_b$, so that the ratios become

$$\frac{C_{\text{coh-hom}}^{(\text{th})}}{C_{\text{ult}}^{(\text{th})}} = 1 - \frac{1}{2n_b} \tag{44}$$

and

$$\frac{C_{\text{coh-het}}^{(\text{th})}}{C_{\text{ult}}^{(\text{th})}} = 1 - \frac{1}{n_b} \tag{45}$$

The approximation in Equation (41) is valid for nonzero n_b. When $n_b = 0$ and $n_s \ll 1$, the ultimate capacity

[7] We use the standard notation $o(x)$ to denote a function that approaches zero faster than x, as x approaches zero, i.e., $\lim_{x\to 0} o(x)/x = 0$.

expression from Equation (24) has the asymptotic expansion

$$C_{\text{ult}} = n_s[1 - \ln(n_s)] + o(n_s) \approx n_s \tag{46}$$

Then, using Equation (27) and Equation (28) we obtain,

$$\frac{C_{\text{coh-hom}}}{C_{\text{ult}}} = \frac{2}{1 - \ln(n_s)} \tag{47}$$

and

$$\frac{C_{\text{coh-het}}}{C_{\text{ult}}} = \frac{1}{1 - \ln(n_s)} \tag{48}$$

for $n_s \ll 1$, both of which converge to zero as n_s goes to zero. Thus both homodyne and heterodyne detection are suboptimal in photon-starved and noiseless communication links.

In the opposite end of the spectrum, when $n_s \gg n_b$, we can simplify the capacity to

$$C_{\text{ult}}^{(\text{th})} = g(n_s) - g(n_b) + n_b \ln(1 + 1/n_s) + o(n_b/n_s) \tag{49}$$

When, in addition, $n_s \gg 1$ is satisfied, this expression further simplifies to

$$C_{\text{ult}}^{(\text{th})} \approx \ln\left(\frac{n_s}{n_b + 1}\right) + 1 - n_b \ln(1 + 1/n_b) \tag{50}$$

We recognize the first term on the right-hand side of Equation (50) as the heterodyne-detection channel capacity in the $n_s \gg \max\{1, n_b\}$ limit. The latter two terms in Equation (50) are independent of the mean received signal photon number n_s, and therefore the ratio of the heterodyne detection capacity and the ultimate capacity approaches unity with increasing n_s. However, in absolute terms, there is a gap between the two capacity expressions that is independent of n_s.[8] Although we have derived Equation (50) for $n_b > 0$, it is valid in the noiseless case as well. Taking the limit of Equation (50) as n_b approaches 0 yields $C_{\text{ult}} \approx \ln(n_s) + 1$, which shows that the ratio of heterodyne-detection capacity and the ultimate capacity approaches 1 when $n_s \gg 1$, but an absolute difference of 1 nat/channel use persists as n_s diverges.

In Figure 12 we have plotted the ultimate capacity expression from Equation (36), along with the approximations Equation (41), Equation (49) and Equation (50), for $n_b = 1$ and $n_b = 10$. We observe that the approximations are in excellent agreement with the exact capacity expression in their regimes of validity.

V. Photon Counting with Multiple Modes

A photon-counting photodetector simply measures the incident photon flux. Hence, using the decomposition given in Section I.B, we observe that all spatiotemporal modes of the impinging field that have nonzero power coupling to the photosensitive surface of the photodetector contribute to the measurement outcome.

[8] Note that $\lim_{x\to 0} \ln(1 + x)/x = 1$ and the function decreases with increasing x. Hence, $1 - n_b \ln(1 + 1/n_b) > 0$ for all $n_b > 0$.

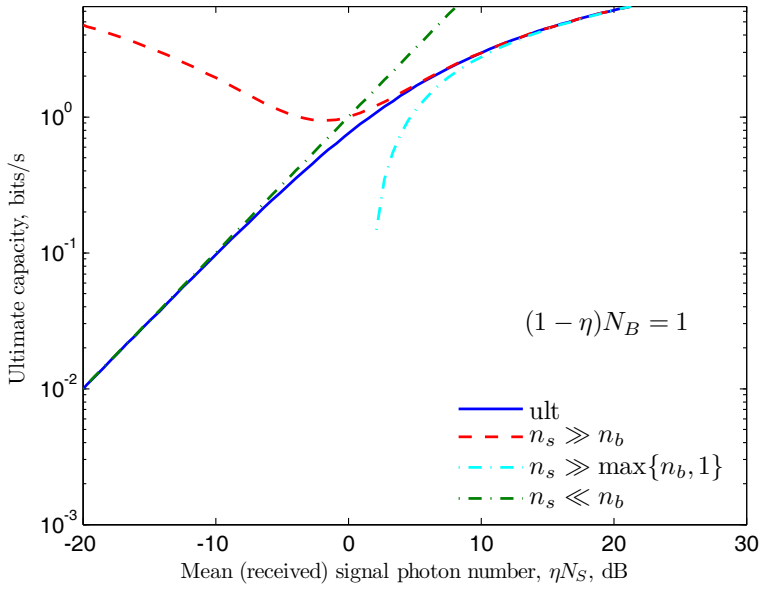

(a) $(1-\eta)N_B = 1$.

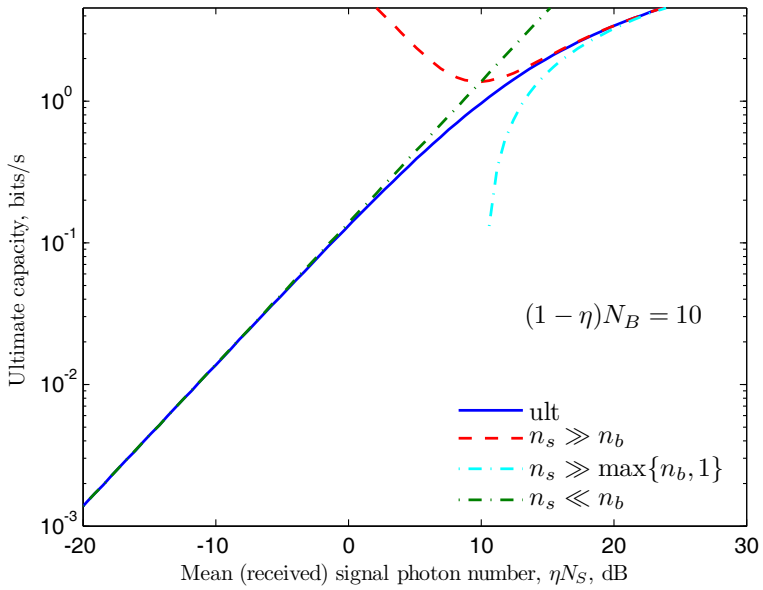

(b) $(1-\eta)N_B = 10$.

Figure 12. (Color online) Asymptotic approximations to the ultimate capacity for the thermal-noise channel ($n_b > 0$). The solid (blue) curve shows the exact expression from Equation (36), the dash-dotted (green) curve is the $n_s \ll n_b$ approximation from Equation (41), the dashed (red) curve is the $n_s \gg n_b$ asymptote from Equation (49), and the dotted (cyan) curve is the $n_s \gg n_b$ and $n_s \gg 1$ approximation from Equation (50).

Consequently, it is desirable to have narrow spectral and spatial optical filters that limit the incident photon flux to that of the modulated signal mode, plus the background photon-flux that occupies this mode. Nevertheless, designing narrow and efficient spatial and spectral filters is a technological challenge, and often there are multiple spatiotemporal modes that have appreciable coupling to the detector's photosensitive surface.

In this section we demonstrate the degradation in single-mode communication performance due to multimode background noise coupling into photon-counting receivers. In particular, let us concentrate on binary on-off keying as our modulation, and let us suppose that the number of modes coupling into the photodetector is K, such that the measurement is given by

$$\hat{N} = \sum_{k=0}^{K-1} \hat{c}_k^\dagger \hat{c}_k \tag{51}$$

where $\hat{c}_0$ denotes the mode with the signal modulation plus thermal noise, and $\hat{c}_k$ for $k = 1, \ldots, K-1$, have no signal (vacuum-state input), but contribute thermal noise.

If $\{\hat{c}_k\}$ are in a thermal product state with equal variances denoted by N, and if $\hat{c}_0$ has mean value $\alpha \in \mathbb{C}$, the photon-counting statistics are given by [2, 24]

$$p(n; K) = \frac{N^n}{(1+N)^{n+K}} L_n^{(K-1)}\left(\frac{-|\alpha|^2}{N(1+N)}\right) e^{-|\alpha|^2/(1+N)} \tag{52}$$

for $n = 0, 1, 2, \ldots$, where $L_n^{(K-1)}(x)$ is the $(K-1)^{\text{th}}$ associated Laguerre polynomial of order n [40].

As in the single-mode case, the channel capacity is a one-dimensional optimization of the mutual information over the pulse transmission probability $p \in (0, 1]$, but, because this mutual information is not in closed form, numerical techniques are used to find the maximum. Figure 13 is a plot of the symbol cost versus the photon-number cost for $(1-\eta)N_B = 0.01$ mean received background photons per mode. As expected, the photon-number efficiency degrades as the number of modes that couple into the photodetector increases.

The $K \gg 1$ limit is often of practical interest because free-space optical communication systems often operate in this regime. Suppose the total measured noise variance is $N' < \infty$, so that each of the K modes has noise variance $N \equiv N'/K$. Then, as $K \to \infty$ with N' fixed, the probability distribution given in Equation (52) approaches a Poisson distribution with mean $N' + |\alpha|^2$, i.e., [2, 24, 39, 41]

$$\lim_{K\to\infty} p(n; K) = (N' + |\alpha|^2)^n e^{-(N'+|\alpha|^2)}/n! \tag{53}$$

for $n = 0, 1, \ldots$. Thus, as K becomes large, the distribution of the photodetected noise is well approximated by a Poisson distribution with the same mean. Figure 13 shows an example for $K = 100$ and $N' = 1$, which confirms that the channel capacity using the Poisson distribution in Equation (53) and the exact capacity obtained from the Equation (52) distribution with $K = 100$ and $N = 0.01$, are nearly identical.

VI. Conclusions

We have provided a brief review of the known results for channel capacities achieved with various modulation (transmitter) and detection (receiver) constraints, as well as the ultimate quantum limits on reliable

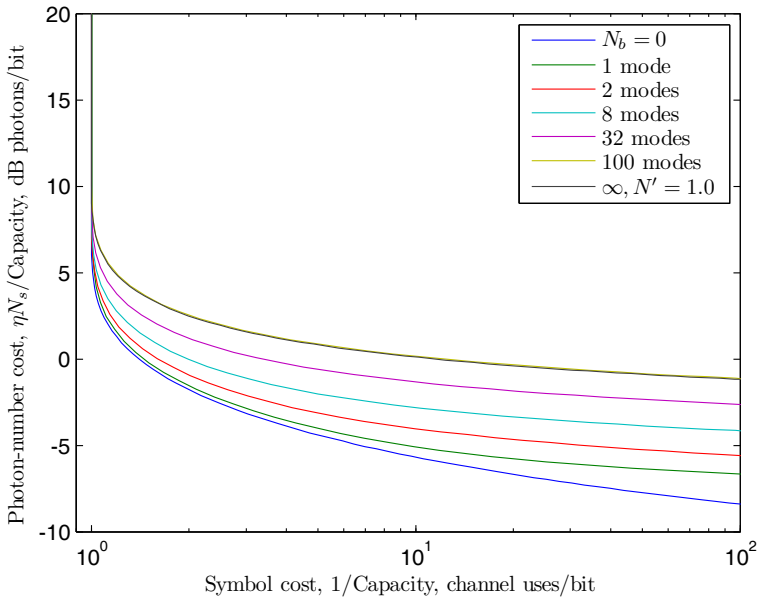

Figure 13. (Color online) Symbol cost versus photon-number cost for OOK plus photon-counting when multiple noise modes, each with mean noise photon number 0.01 photons/mode, couple into the photodetection measurement. The curve labeled ∞ denotes Poisson noise statistics with total mean photon number $N' = 1$, which shows that aggregate photon-number statistics of multimode noise with large K (e.g., $K = 100$ modes with 0.01 photons/mode) is well-modeled as a Poisson random variable having the same mean total photon number.

communication of classical information. The ultimate capacity is achievable with classical-state light, namely coherent states, but the corresponding optimal receivers are yet to be determined. Plots indicate that there are several decibels of potential gain (per mode) from pursuing the optimal receivers that achieve the ultimate capacity when the background radiation (per mode) is negligible.

An important outcome of the results presented in Section II is that binary phase-shift keying (BPSK), in combination with the optimal measurement (as yet to be determined), is near-optimal in photon-starved channels. Furthermore, its channel capacity exceeds that of on-off keying (OOK), in combination with either photon-counting photodetectors or even the optimal measurement. The current technology development for laser transmitters with high peak-to-average power ratios is geared towards approaching the capacity with pulsed (intensity) modulations (such as on-off keying or pulse position modulation) in combination with high-bandwidth photon-counting detectors. The results given in Section II provide a framework for comparing different modulation and receiver configurations, and suggest that in photon-starved links binary antipodal signaling (binary phase-shift keying) using phase-coherent lasers, in combination with an optimal receiver to decode the information encoded with such modulation, performs very close to the ultimate capacity of the channel dictated by quantum mechanics. On-off keying with the optimal receiver performs strictly worse than the former configuration, and on-off keying with photon counting performs even worse than the former two. Therefore, future technology development of phase-stable (continuous-wave) lasers, and research into near-optimal receivers to detect phase-modulated waveforms can enable optical communication at higher rates, or at lower (power and bandwidth) cost than the current state of the art. Furthermore, phase modulation offers an alternative to the high peak-to-average power ratio required by on-off keying, and therefore it may notably

expand the trade space of viable laser transmitter technologies.

The results for thermal-state channels are, to date, limited. The ultimate capacity had been, until recently, a conjecture subject to the proof of either the minimum output entropy conjecture, or the entropy photon-number inequality conjecture. Nevertheless, very recently both of these conjectures have been proven true, and the channel capacity conjecture has been resolved. As we have reviewed in this article, the capacity-achieving transmitter states are classical coherent states, but the optimal measurement is not yet known. Our comparison of several structured transmitter and receivers has shown that the optimal (isotropic Gaussian) modulation plus heterodyne or homodyne detection outperforms OOK plus photon-counting, except possibly in the limit of very small mean signal photon numbers. We have also shown that heterodyne detection is near-optimal at high mean signal photon numbers. Homodyne detection becomes near-optimal only in the low signal and high background case.

Heterodyne and homodyne detection are inherently single spatial mode, because the measured field is mode-matched to the local oscillator's spatial mode, and can be made single temporal mode by matched filtering the photocurrent. On the other hand, in photon-counting receivers, all modes of the incident field that have nonzero coupling to the photosensitive surface of the photodetector contribute to the measurement outcome. Whereas auxiliary unexcited (vacuum-state) modes are of no consequence, in the presence of thermal noise, extra noise modes can significantly impair performance. Therefore, it is relevant that the spatiotemporal auxiliary mode coupling is minimized in photon-counting receivers. Temporal modes can be eliminated via spectral filtering prior to photodetection, and spatial modes can be limited by reducing the detector's field-of-view. The number of noise modes that affect a photodetector is approximately given by the product of the photodetector integration time and the optical bandwidth. Most photon-counting receivers operate with many auxiliary noise modes, each contributing some background radiation. As we have shown in this article, this can have a significant impact on the channel capacity.

Several questions for the thermal-noise communication channel remain open. For example, it is of practical interest to determine if BPSK in combination with the optimal measurement still approaches the ultimate capacity of the thermal-noise channel. Similarly, the performance of OOK with the optimal measurement, relative to the ultimate capacity and the capacity achieved with photon counting is of interest. These comparisons will quantify the gains from developing optimal receivers, and will improve our understanding of good modulation formats in the presence of (background) noise.

We should take a moment to acknowledge that the analysis in this article does not account for atmospheric turbulence, which cannot be ignored in terrestrial, space-to-Earth or Earth-to-space communication links. Turbulence is caused by the nonuniform temperature distribution of the atmosphere, which results in a nonuniform refractive index profile [42]. The impact of turbulence in a communication system is fading (sometimes also referred to as scintillation), due to the constructive and destructive interference of different plane-wave components of the field impinging on the receiver aperture, and, beam spread and angular spread, due to the distortion in the phase front. These impairments do not preclude reliable communication; however, the degree to which they impact different communication technologies vary widely. Therefore, an analysis—paralleling that presented in this article for free-space communication—should be carried out for channel capacity in the presence of turbulence.

Finally, it is worthwhile to emphasize that these results are for single-mode communication. Multiple temporal modes may be utilized in communication links that have a time-bandwidth product greater than unity. Multiple spatial modes may be utilized in communication link geometries that are not deep in the far-field [14]. As implied by the mode decomposition of the free-space propagation kernel, multiple (spatial and/or temporal) modes could be conceivably utilized to convey information over effective parallel channels, each with a different coupling coefficient η. The optimal photon number allocation in each of these parallel channels, the gains associated with multimode communication, and the complexity of the transmitters and receivers, are relevant questions that should be answered in order to delineate the full potential of optical communication.

References

[1] R. Loudon, *The Quantum Theory of Light*. New York: Oxford Univ., 3rd ed., 2000.

[2] L. Mandel and E. Wolf, *Optical Coherence and Quantum Optics*. Cambridge: Cambridge Univ., 1995.

[3] M. A. Nielsen and I. L. Chuang, *Quantum Computation and Quantum Information*. Cambridge: Cambridge Univ., 2000.

[4] C. E. Shannon, "A Mathematical Theory of Communication," *Bell Systems Technical Journal*, vol. 27, pp. 379–423, 1948.

[5] Y. Yamamoto and H. A. Haus, "Preparation, Measurement and Information Capacity of Optical Quantum States," *Reviews of Modern Physics*, vol. 58, pp. 1001–1020, 1986.

[6] C. M. Caves and P. D. Drummond, "Quantum Limits on Bosonic Communication rates," *Reviews of Modern Physics*, vol. 66, pp. 481–537, 1994.

[7] D. M. Boroson, "Optical Communications: A Compendium of Signal Formats, Receiver Architectures, Analysis Mathematics and Performance Comparisons," in *MIT Lincoln Laboratory Report*, vol. 60-1054, 2005.

[8] D. M. Boroson, "A Survey of Technology-Driven Capacity Limits for Free-Space Laser Communications," in *Proceedings of the SPIE*, vol. 6709, p. 670918, 2007.

[9] T. M. Cover and J. A. Thomas, *Elements of Information Theory*. New Jersey: Wiley, 2nd ed., 2006.

[10] A. S. Holevo, "The Capacity of the Quantum Channel with General Signal States," *IEEE Transactions on Information Theory*, vol. 44, pp. 269–273, 1998.

[11] V. Giovannetti, S. Guha, S. Lloyd, L. Maccone, J. H. Shapiro, and H. P. Yuen, "Classical Capacity of the Lossy Bosonic Channel: The Exact Solution," *Physical Review Letters*, vol. 92, p. 027902, 2004.

[12] V. Giovannetti, S. Guha, S. Lloyd, L. Maccone, J. H. Shapiro, B. J. Yen, and H. P. Yuen, "Classical Capacity of Free-Space Optical Communication," *Quantum Information and Computation*, vol. 4, pp. 489–499, 2004.

[13] H. P. Yuen and J. H. Shapiro, "Optical Communication with Two-Photon Coherent States—Part I: Quantum State Propagation and Quantum Noise Reduction," *IEEE Transactions on Information Theory*, vol. 24, pp. 657–668, 1978.

[14] J. H. Shapiro, S. Guha, and B. I. Erkmen, "Ultimate Channel Capacity of Free-Space Optical Communications [Invited]," *Journal of Optical Networking*, vol. 4, pp. 501–516, 2005.

[15] J. H. Shapiro, "The Quantum Theory of Optical Communications," *to be published in IEEE Journal of Selected Topics in Quantum Electronics*, 2010.

[16] D. Slepian, "Analytic Solution of Two Apodization Problems," *Journal of the Optical Society of America*, vol. 55, pp. 1100–1115, 1965.

[17] H. P. Yuen and M. Ozawa, "Ultimate Information Carrying Limit of Quantum Systems," *Physical Review Letters*, vol. 70, pp. 363–366, 1993.

[18] Y. C. Eldar and G. D. Forney Jr., "On Quantum Detection and the Square-Root Measurement," *IEEE Transactions on Information Theory*, vol. 47, pp. 858–872, 2001.

[19] P. Hausladen, R. Jozsa, B. Schumacher, M. Westmoreland, and W. K. Wooters, "Classical Information Capacity of a Quantum Channel," *Physical Review A*, vol. 54, pp. 1869–1876, 1996.

[20] B. Schumacher and M. D. Westmoreland, "Sending Classical Information via Noisy Quantum Channels," *Physical Review A*, vol. 56, pp. 131–138, 1997.

[21] M. Osaki, M. Ban, and O. Hirota, "Derivation and Physical Interpretation of the Optimum Detection Operators for Coherent-State Signals," *Physical Review A*, vol. 54, pp. 1691–1701, 1996.

[22] M. Sasaki, T. Sasaki-Usuda, M. Izutsu, and O. Hirota, "Realization of Collective Decoding of Code-Word States," *Physical Review A*, vol. 58, pp. 159–164, 1998.

[23] R. H. Kingston, *Detection of Optical and Infrared Radiation*. New York: Springer-Verlag, 1978.

[24] R. M. Gagliardi and S. Karp, *Optical Communications*. New York: Wiley, 1976.

[25] J. H. Shapiro, "Quantum Noise and Excess Noise in Optical Homodyne and Heterodyne Receivers," *IEEE Journal of Quantum Electronics*, vol. QE-21, pp. 237–250, 1985.

[26] J. H. Shapiro, H. P. Yuen, and J. A. M. Mata, "Optical Communication with Two-Photon Coherent States—Part II: Photoemissive Detection and Structured Receiver Performance," *IEEE Transactions on Information Theory*, vol. 25, pp. 179–192, 1979.

[27] J. H. Shapiro and S. R. Shepard, "Quantum phase measurement: a system-theory perspective," *Physical Review A*, vol. 43, pp. 3795–3818, 1991.

[28] A. Martinez, "Spectral Efficiency of Optical Direct Detection," *Journal of the Optical Society of America A*, vol. 24, pp. 739–749, 2007.

[29] S. Guha, *Multiple-User Quantum Information Theory for Optical Communication Channels*. PhD thesis, Massachusetts Institute of Technology, Cambridge, MA, 2008.

[30] S. J. Dolinar, "An Optimum Receiver for the Binary Coherent State Quantum Channel," in *MIT Research Laboratory of Electronics Quarterly Progress Report*, vol. 111, pp. 115–120, 1973.

[31] S. Verdu, "On Channel Capacity per Unit Cost," *IEEE Transactions on Information Theory*, vol. 36, pp. 1019–1030, 1990.

[32] N. S. Kopeika and J. Bordogna, "Background Noise in Optical Communication Systems," in *Proceeding of the IEEE*, vol. 58, pp. 1571–1577, 1970.

[33] F. Capasso, R. Paiella, R. Martini, R. Colombelli, C. Gmachl, T. L. Myers, M. S. Taubman, R. M. Williams, C. G. Bethea, K. Unterrainer, H. Y. Hwang, D. L. Sivco, A. Y. Cho, A. M. Sergent, H. C. Liu, and E. A. Whittaker, "Quantum Cascade Lasers: Ultrahigh-Speed Operation, Optical Wireless Communication, Narrow Linewidth, and Far-Infrared Emission," *IEEE Journal of Quantum Electronics*, vol. 38, pp. 511–532, 2002.

[34] M. J. Fitch and R. Osiander, "Terahertz Waves for Communications and Sensing," in *Johns Hopkins APL Technical Digest*, vol. 25, pp. 348–355, 2004.

[35] V. Giovannetti, S. Guha, S. Lloyd, L. Maccone, and J. H. Shapiro, "Minimum Output Entropy of Bosonic Channels: A Conjecture," *Physical Review A*, vol. 70, p. 032315, 2004.

[36] S. Guha, J. H. Shapiro, and B. I. Erkmen, "Capacity of the Bosonic Wiretap Channel and the Entropy Photon-Number Inequality," in *Proceedings of the 2008 International Symposium on Information Theory*, pp. 91–9–5, 2008.

[37] S. Lloyd, V. Giovannetti, L. Maccone, N. J. Cerf, S. Guha, R. Garcia-Patron, S. Mitter, S. Pirandola, M. B. Ruskai, J. H. Shapiro, and H. Yuan, "Proof of the Bosonic Minimum Output Entropy Conjecture," *e-print:* `arXiv:0906.2758v1 [quant-ph]`, 2009.

[38] S. Lloyd, V. Giovannetti, L. Maccone, S. Pirandola, and R. Garcia-Patron, "Minimum Output Entropy of Gaussian Channels," *e-print:* `arXiv:0906.2762v1 [quant-ph]`, 2009.

[39] D. L. Snyder, *Random Point Processes*. New York: Wiley, 1975.

[40] L. C. Andrews, *Special Functions of Mathematics for Engineers*. New York: McGraw-Hill, 2nd ed., 1992.

[41] G. R. Osche, *Optical Detection Theory for Laser Applications*. New Jersey: Wiley, 2002.

[42] L. C. Andrews and R. L. Phillips, *Laser Beam Propagation through Random Media*. Bellingham: SPIE, 2nd ed., 2005.